

Article

## Compressive Behaviors of Micropillar Patterns Made of PDMS Material using the Finite Element Method

Thitikan Pakawan<sup>1,a</sup>, Tumrong Puttapitukporn<sup>1,b,\*</sup>, Nithi Atthi<sup>2,c</sup>, Witsaroot Sripumkhai<sup>2</sup>, Pattaraluck Pattamang<sup>2</sup>, Nipapan Klunngien<sup>2</sup>, and Wutthinan Jeamsaksiri<sup>2</sup>

<sup>1</sup> Department of Mechanical Engineering, Faculty of Engineering, Kasetsart University, Bangkok 10900, Thailand

<sup>2</sup> Thai Microelectronics Center (TMEC), National Electronics and Computer Technology Center (NECTEC), Chachoengsao 24000, Thailand

E-mail: <sup>a</sup>thitikan.work@gmail.com, <sup>b</sup>fengtop@ku.ac.th (Corresponding author), <sup>c</sup>nithi.atthi@nectec.or.th

**Abstract.** Hydrophobic surface is a surface having the ability of water repellent which is frequently coated on medical devices and marine structures. This hydrophobic surface can fabricate from micro-pattern sheets consisting of groups of micropillars arranged into unique micro-patterns which are normally made of low surface energy materials. Thai Microelectronics Center (TMEC) has fabricated micropillar sheets from PDMS for various micropillar array patterns from soft lithography techniques. However, these micropillar sheets were relatively weak under pushing forces. This research aimed to understand compressive behaviors of rectangular prism micropillars having different aspect ratios (ratio of width to length of a rectangular cross-section) and micro-patterns consisting of micropillars having rectangular cross-section and square cross-section by using ANSYS Mechanical APDL program. We found that the aspect ratio of prism micropillars had not influences on both elastic stiffness and compressive strength under compressive loading. The lateral collapse of micropillars were observed on all micro-patterns during compressive loading. Furthermore, the sharklet micro-pattern had the highest compressive strength with maximum compressive pressure of 9.87 kPa. Finally, as loading contact area of micro-patterns increases, the compressive strength increases while the water contact angle decreases.

**Keywords:** Hydrophobic surface, polydimethylsiloxane, micro-pattern, finite element analysis, ANSYS.

ENGINEERING JOURNAL Volume 25 Issue 1

Received 13 May 2020

Accepted 24 November 2020

Published 31 January 2021

Online at <https://engj.org/>

DOI:10.4186/ej.2021.25.1.69

## 1. Introduction

Biofouling on surfaces, such as virus, bacteria, and disease on medical equipment surface and food applications have been a health risk. Moreover, biofouling of seaweed, bacteria and barnacles on marine engineering structures and tools have been a significant impact on structural damage [1]. To prevent biofouling on these surfaces, superhydrophobic films are often coated on medical equipment or marine engineering structures. Polydimethylsiloxane (PDMS) materials are generally used to fabricate superhydrophobic surfaces because of their low surface energy, non-toxic, non-flammable and good biocompatibility [2]. The hydrophobic properties are regulated by the water wetting angle of the surface. Gomes, Souza and Silva [3] classified the wettability property of surfaces by a water contact angle. Firstly, if the water contact angle is under 90 degrees, it is called a hydrophilic surface. Secondly, if the water contact angle is between 90 to 150 degrees, it is called a hydrophobic surface. Thirdly, if the water contact angle is greater than 150 degrees, it is called a superhydrophobic surface. This surface can improve hydrophobicity by creating rough surface consisting of micro- or nano- structures on substrate surfaces [4]. The rough surface can be prepared from cultivating micropillars on the substrate surfaces; however, micropillars could experience self-mating micropillars upon the pushing force. As result, hydrophobic properties would blunder away [5]. Microstructure can be robust if micropillars are designed with unique sizes and shapes. For this reason, many researches have focused studies not only on micro- and nano-patterns which prevent biofouling but also on mechanical behaviors of hydrophobic surfaces under various loading conditions. Graham and Cady [6] found that the sharklet pattern on hydrophobic surface could prevent biofouling. Rahmawan et al. [7] fabricated the PUA cylinder-shaped micropillars with silica particles on top of micropillar's head and compared their shear adhesion strength to non-silica particles. The authors found that the micropillars with silica particles showed higher shear adhesion strength than micropillars without particles. Atthi et al. [8] studied effects of various asperity shapes on superhydrophobic surfaces. The authors found that the pentagonal pillars with square and hexagonal arrays had highest water contact angle of 155.9 degrees. Atthi et al. [9] studied effects of various PDMS micro-structures on hydrophobic and antifouling properties. The authors found that the circular rings with eight stripe supporters (C-RESS) pattern illustrated highest durability that can robust to collapse under external loads. Lu et al. [10] studied effects of pattern size on micro-patterns to prevent bacteria adhesion. The authors found that the pattern size significantly reduced bacteria adhesion, when the pattern size was smaller than the bacteria size, the micro-pattern had better capability to prevent bacteria adhesion. Chebolu et al. [11] studied effects of micro-nano scale patterns made of PDMS material on resisting bacteria activity. The authors found that the highest bacteria adhesion was found on a smooth PDMS.

Furthermore, the square and circular micropillars illustrated better resistance to bacteria adhesion. Pakawan et al. [12] studied effects of decreasing the substrate thicknesses on mechanical behaviors of PDMS micropillar sheets under compressive loading in ANSYS Mechanical APDL program. The authors found that the compressive strength and the lateral collapse of micropillars depended on substrate thickness. As the substrate thickness decreased, the compressive strength decreased while the elastic stiffness increased. Furthermore, the micropillar sheet without the substrate did not experience lateral collapse under the compressive load. Thanakhun and Puttakitkorn [13] studied structural behaviors of micropillars fabricated from a core made of PUA material coated with a PDMS material and compared their lateral strength under shear loadings in ANSYS Mechanical APDL program. The authors found that the PUA core coated with 100 nm-thick PDMS micropillar illustrated better lateral strength than pure PDMS micropillar. Cheng et al. [14] studied the sensing device using liquid crystal in micropillar arrays for supporting structure. The authors found that liquid crystal thin film supported in the micropillar arrays were robust and withstand to gravitational forces and mechanical shock. Johari and Shyan [15] used the finite element method to study effect of height and diameter of the cylindrical micropillar made of PDMS material under shear forces. The authors found that deformation increases when micropillar height increased and micropillar diameter decreased. Singh et al. [16] studied deformation of taper and tapered-free micropillars under compressive loading using the finite element method. The FE results showed that straight micropillars had more compressive strength than tapered micropillars. Du et al. [17] analysed the reaction forces in micro-pattern with square micropillars made of PDMS material by using finite element method. Their FE results were compared with the experiment data. The FE results of reaction forces correlated well with the experimental data. Oyunbaatar et al. [18] studied contraction forces of PDMS micropillar arrays with and without grooves on the top of micropillar by using the finite element method. The FE results showed that micropillar with grooves had more contraction force than micropillar without grooves. Liu et al. [19] analysed the automated demolding process of PDMS micropillars with aspect ratio of 6 in LS-DYNA program. The authors found that the FE results correlated well with the experimental data and the peel demolding process had not showed a significant effect on the low aspect ratio of micropillars. Xu et al. [20] used the finite element method to study mechanical properties of SU-8 micropillars under both compressive and nanoindentation test in ABAQUS program. The authors found that Young's modulus decreased as diameter of micropillar increased. Furthermore, the yield strength increased as diameter of micropillar increased.

This research was extended work of Pakawan et al. [12] which aimed to understand compressive behaviors of rectangular prism micropillars having different aspect ratios (ratio of width to length of a rectangular cross-

section) and micro-patterns consisting of micropillars having rectangular cross-section and square cross-section in ANSYS Mechanical APDL program.

## 2. Theory

The hyperelastic constitutive models are developed to describe a nonlinear stress-strain relationship which expresses abilities of materials to experience large deformation under small loads and to recover their initial shape upon unloading [21]. In this research, the accurate constitutive model of PDMS under compressive loading was the Mooney-Rivlin 5 parameters [12]. The typical strain energy density function ( $W$ ) can be written in terms of the invariants ( $\bar{I}$ ) and stretch ratios ( $\lambda$ ). The invariants can be written as

$$\bar{I}_1 = \lambda_1^2 + \lambda_2^2 + \lambda_3^2 \quad (1)$$

$$\bar{I}_2 = \lambda_1^2 \lambda_2^2 + \lambda_2^2 \lambda_3^2 + \lambda_1^2 \lambda_3^2 \quad (2)$$

$$\bar{I}_3 = \lambda_1^2 \lambda_2^2 \lambda_3^2 \quad (3)$$

The stretch ratio in the  $i$ -direction can be written as

$$\lambda_i = \frac{L_i}{(L_0)_i} = 1 + \varepsilon_i \quad (4)$$

where  $(L_0)_i$ ,  $L_i$  and  $\varepsilon_i$  are the initial length, the instantaneous length and the engineering strain in the  $i$ -direction respectively. The principal stress ( $\sigma$ ) in the  $i$ -direction is derived from the strain energy function as

$$\sigma_i = \lambda_i \frac{\partial W}{\partial \lambda_i} \quad (5)$$

### 2.1 Mooney-Rivlin 5 parameters

The Mooney-Rivlin model is developed from Neo-Hookean model. The strain energy density function of Mooney-Rivlin model depends on the 1<sup>st</sup> and 2<sup>nd</sup> invariants and can be written as in Eq. (6).

$$\begin{aligned} W = & C_{10}(\bar{I}_1 - 3) + C_{01}(\bar{I}_2 - 3) \\ & + C_{20}(\bar{I}_1 - 3)^2 + C_{11}(\bar{I}_1 - 3)(\bar{I}_2 - 3) \\ & + C_{02}(\bar{I}_2 - 3)^2 + \frac{1}{D}(J - 1)^2 \end{aligned} \quad (6)$$

where  $W$  is strain energy density function,  $C_{10}$ ,  $C_{01}$ ,  $C_{20}$ ,  $C_{11}$  and  $C_{02}$  are material constants,  $\bar{I}_1$  is the 1<sup>st</sup> invariant,  $\bar{I}_2$  is the 2<sup>nd</sup> invariant,  $D$  is a material incompressibility constant and  $J$  is elastic volumetric ratio.

## 3. Methodology

Thai Microelectronics Center (TMEC) fabricates micropillar sheets from PDMS material (having ratio of a PDMS monomer to a curing agent ratio of 10:1) for various micropillar array patterns from soft lithography techniques. To study effects of a pillar's cross section areas on its loading respond, the rectangular prism micropillars having different aspect ratios (ratio of width to length of rectangular cross-sections) as shown in Fig. 1. The micropillar array patterns which consisted of F3, F4, F8 and F13 pattern respectively as shown in Fig. 2-5. These micro-patterns are rectangular prism micropillars (F3 and F4 patterns) and square prism micropillars (F8 pattern). The sharklet pattern is F13. These micro-patterns were modelled in ANSYS Mechanical APDL program. Table 1 illustrates laboratory testing of water contact angles (WCA) of micro-patterns. The hyperelastic material constants acquired from [12].

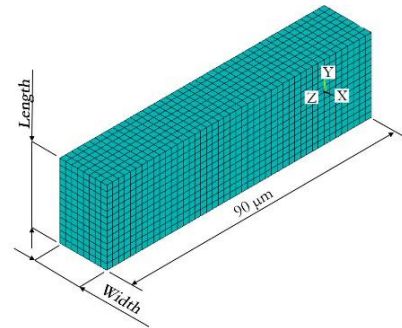


Fig. 1 Micropillar without substrate.

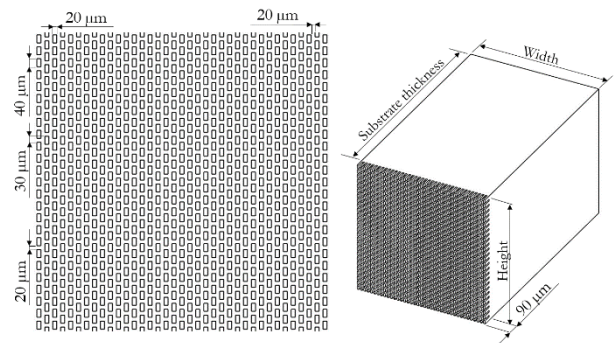


Fig. 2. Dimension of F3 pattern.

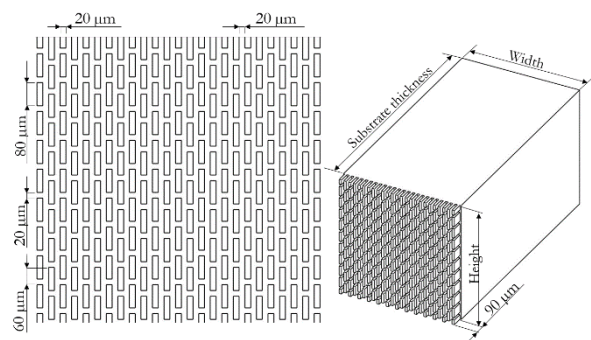


Fig. 3. Dimension of F4 pattern.

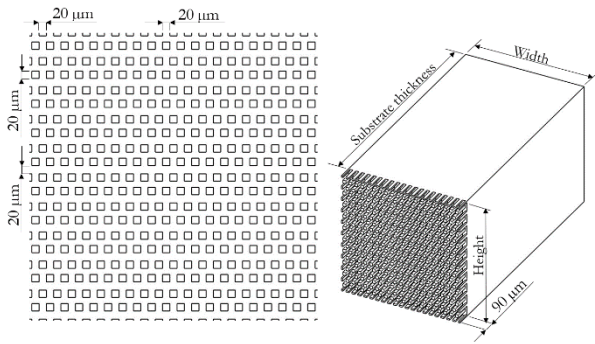


Fig. 4. Dimension of F8 pattern.

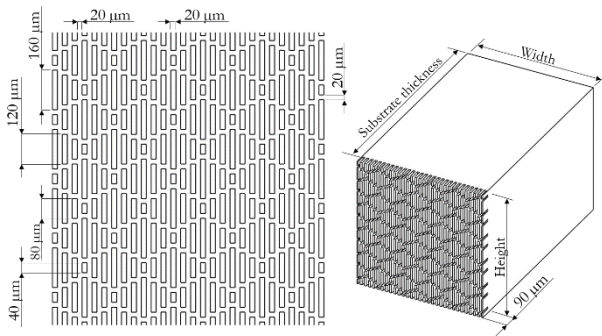
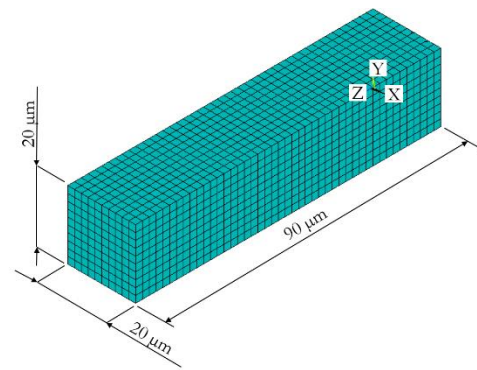


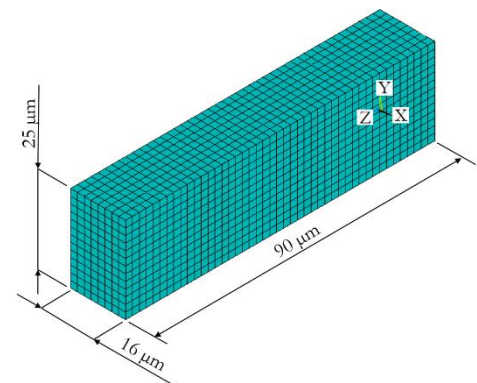
Fig. 5. Dimension of F13 pattern.

The FE models of micropillars having different aspect ratios of rectangular cross section areas consisted of  $20\ \mu\text{m} \times 20\ \mu\text{m}$  (ratio of 1:1),  $16\ \mu\text{m} \times 25\ \mu\text{m}$  (ratio of 1:1.56) and  $10\ \mu\text{m} \times 40\ \mu\text{m}$  (ratio of 1:4) as shown in Fig. 6. The FE models were meshed by using SOLID186 elements which were 20-nodes structural solid elements which have 3 translations in the x, y and z directions for each node. The number of elements of each FE models were 4,500, 4,680 and 4,500 elements respectively. Their boundary conditions were that all nodes on the bottom surface were fixed in all degree of freedom while all nodes on the top surface were coupled the displacement in the z-direction. For reducing FE computational time and evaluating convergence of FE results, the replicas of micropillar array patterns were studied. The FE models of F3 pattern consisted of 1, 56, 70 and 84 micropillars respectively as shown in Fig. 7. The FE models of F4 pattern consisted of 1, 56, 70 and 84 micropillars as shown in Fig. 8. The FE models of F8 pattern consisted of 1, 28, 56 and 70 micropillars as shown in Fig. 9. The FE models of F13 pattern consisted of 1, 6, 10 and 12 cells as shown in Fig. 10. Furthermore, all replicas of micropillar array patterns were modeled on  $150\ \mu\text{m}$  thick substrate in which the substrate had height and width long enough for focusing only on interactions between micropillars as listed in Table 2-5. The FE models were meshed using SOLID186 elements. The number of elements of each FE models as listed in Table 6-9. The boundary conditions of each FE model were that all nodes on the top surface of micropillars were coupled the displacement in the z-direction while all nodes on bottom surface of the substrate were fixed in all degree of freedom. The surface-

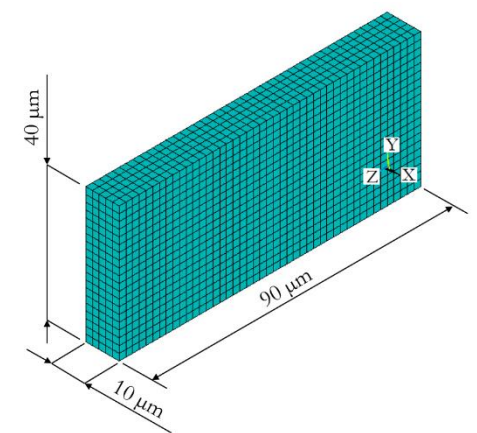
to-surface contact without friction was applied to each micropillar. The accurate constitutive model of PDMS was Mooney-Rivlin 5 parameters [12] in which material constants were illustrated in Table 10.



(a)

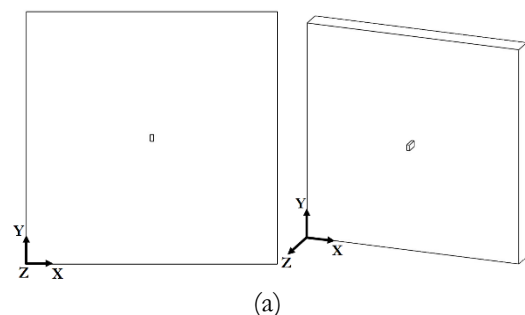


(b)



(c)

Fig. 6. FE models of micropillar for aspect ratio of (a) 1:1, (b) 1:1.56 and (c) 1:4.



(a)

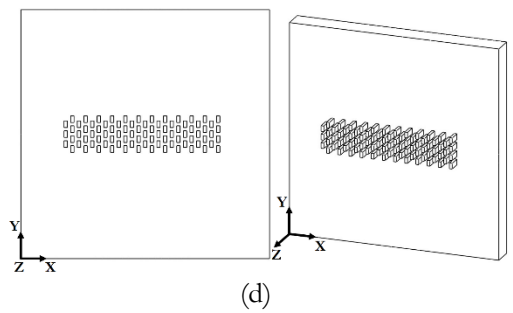
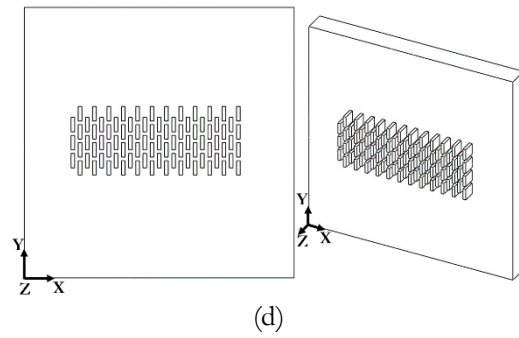
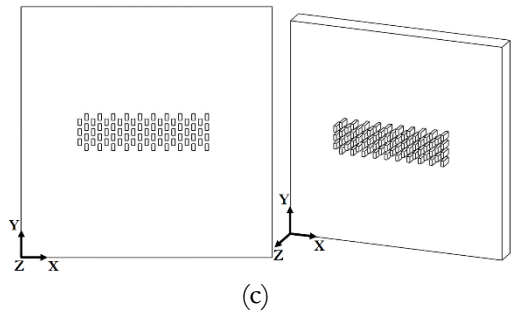
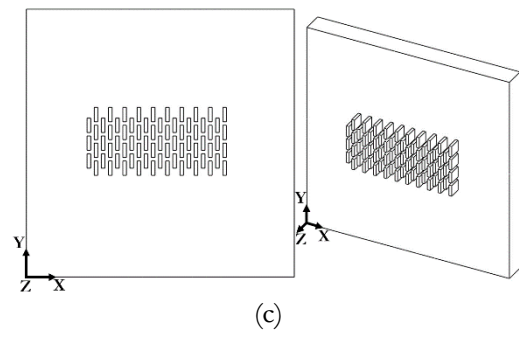
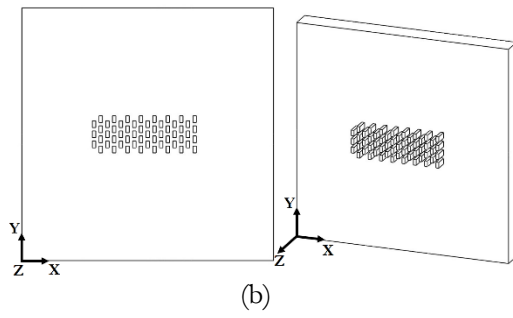


Fig. 8. 3D models of F4 pattern for (a) one micropillar, (b) 56 micropillars, (c) 70 micropillars and (d) 84 micropillars.

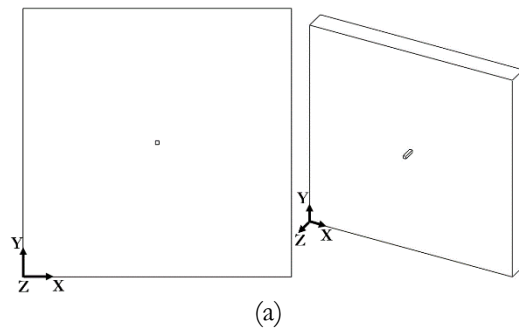
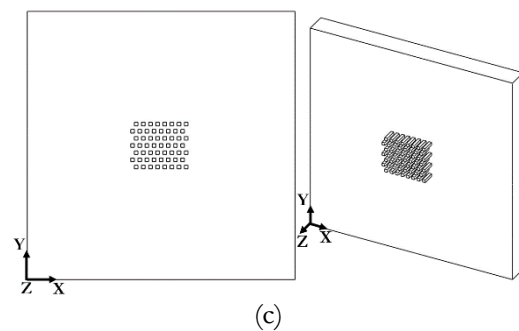
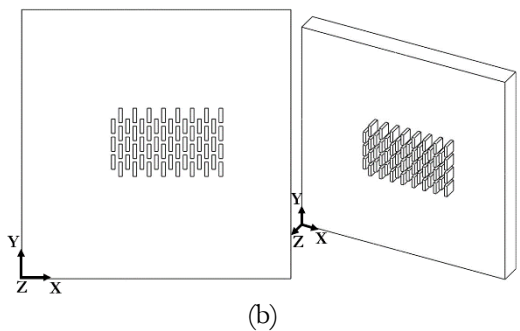
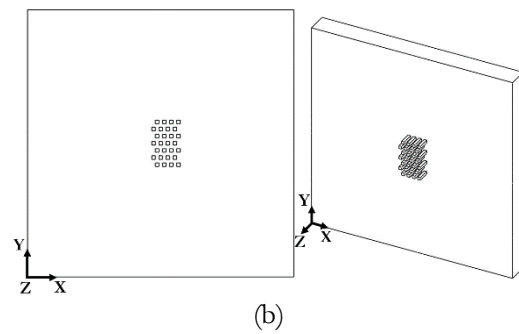
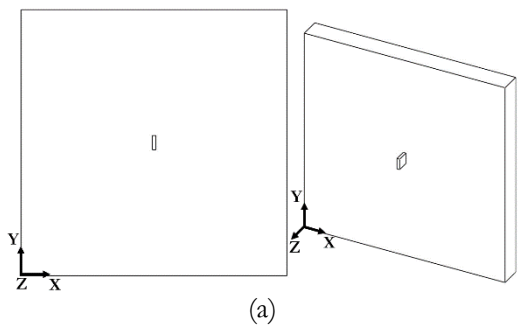


Fig. 7. 3D models of F3 pattern for (a) one micropillar, (b) 56 micropillars, (c) 70 micropillars and (d) 84 micropillars.



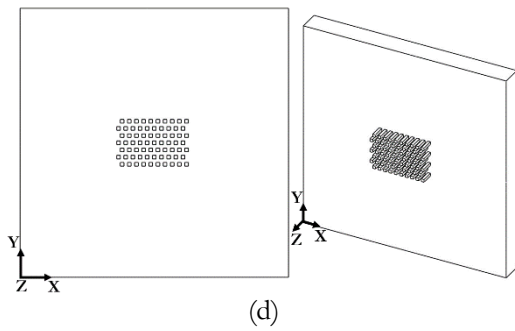


Fig. 9. 3D models of F8 pattern for (a) one micropillar, (b) 28 micropillars, (c) 56 micropillars and (d) 70 micropillars.

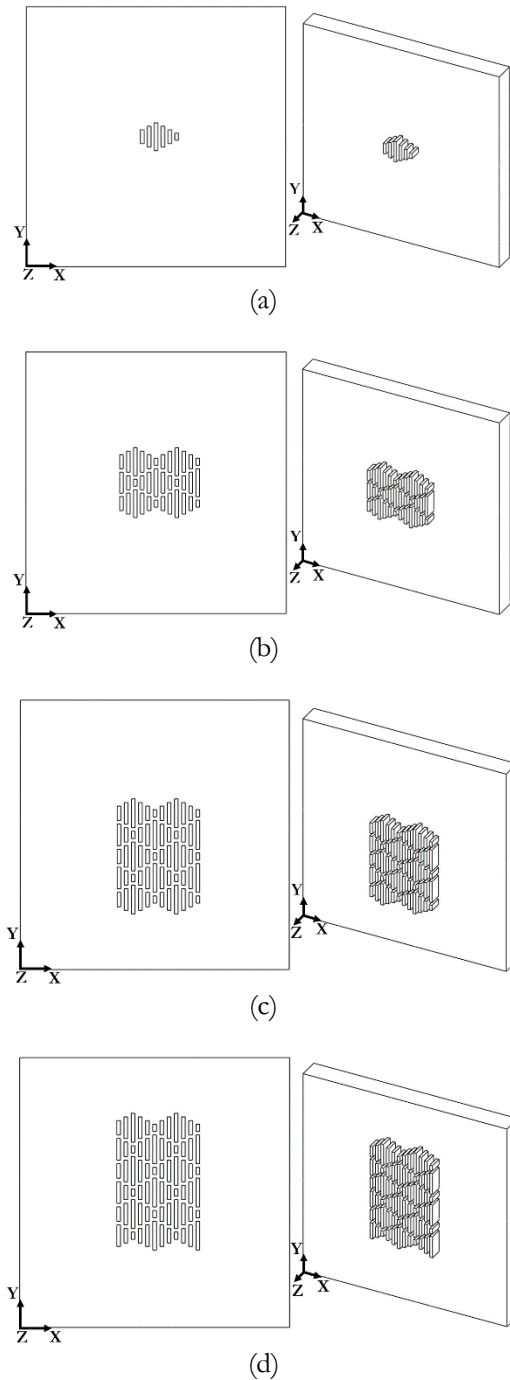


Fig. 10. 3D models of F13 pattern for (a) 1 cell, (b) 6 cells, (c) 10 cells and (d) 12 cells.

Table 1. Water contact angles (WCA) of micro-patterns.

Micro-patterns	WCA (degree)
F3	139.6
F4	135.6
F8	143.6
F13	134.7

Table 2. FE models of F3 pattern.

Number of micropillars	Width ( $\mu\text{m}$ ) x Height ( $\mu\text{m}$ )
1	700 x 700
56	1,300 x 1,300
70	1,300 x 1,300
84	1,300 x 1,300

Table 3. FE models of F4 pattern.

Number of micropillars	Width ( $\mu\text{m}$ ) x Height ( $\mu\text{m}$ )
1	1,200 x 1,200
56	1,200 x 1,200
70	1,200 x 1,200
84	1,200 x 1,200

Table 4. FE models of F8 pattern.

Number of micropillars	Width ( $\mu\text{m}$ ) x Height ( $\mu\text{m}$ )
1	1,500 x 1,500
28	1,500 x 1,500
56	2,000 x 2,000
70	2,000 x 2,000

Table 5. FE models of F13 pattern.

Number of cells	Width ( $\mu\text{m}$ ) x Height ( $\mu\text{m}$ )
1	1,800 x 1,800
6	1,800 x 1,800
10	1,800 x 1,800
12	1,800 x 1,800

Table 6. The number of elements of F3 pattern.

Number of micropillars	Number of elements
1	4,972
56	28,852
70	31,948
84	35,044

Table 7. The number of elements of F4 pattern.

Number of micropillars	Number of elements
1	14,544
56	179,712
70	211,104
84	242,496

Table 8. The number of elements of F8 pattern.

Number of micropillars	Number of elements
1	22,536
28	25,776
56	47,020
70	48,892

Table 9. The number of elements of F13 pattern.

Number of cells	Number of elements
1	34,452
6	45,756
10	54,900
12	59,400

Table 10. The material constants of Mooney-Rivlin 5 parameters.

Material constants	Value
$C_{10}$	-0.16808
$C_{01}$	0.23398
$C_{11}$	-2.54487
$C_{20}$	2.09914
$C_{02}$	0.78043
D	0

#### 4. Results and Discussion

In analyzing aspect ratio of a rectangular cross section of prism-micropillars, we found that the aspect ratio did not influence on both elastic stiffness and compressive strength of the micropillar as shown in Fig. 11-12. Figure 13 shows contour plot of deformation in z-direction. Figure 14 shows contour plots of von-mises stress for various aspect ratios. Here, the maximum von-mises stress occurring on the fixed surface. Figures 15-18 show the plots of compressive force and vertical displacement of F3, F4, F8 and F13 patterns respectively. We found convergence on all FE results when the number of micropillars was high enough to capture interactions between micropillars which were 84 micropillars for F3 and F4 patterns, 70 micropillars for F8 pattern and 12 cells for F13 pattern. Their contour plot of deformation in the z-direction as shown in Fig. 19. Moreover, the compressive strength of various micropillar patterns were

compared and the plot of compressive pressure and vertical displacement for various micropillar patterns were shown in Fig. 20. The maximum compressive pressure were 7.73 kPa, 9.79 kPa, 5.45 kPa and 9.87 kPa for F3, F4, F8 and F13 patterns respectively. We found that F13 pattern had the highest in both elastic stiffness and the compressive strength since it had the highest loading contact area. For all micro-patterns, the collapse of micro patterns were found when the deformation was around 5  $\mu\text{m}$ .

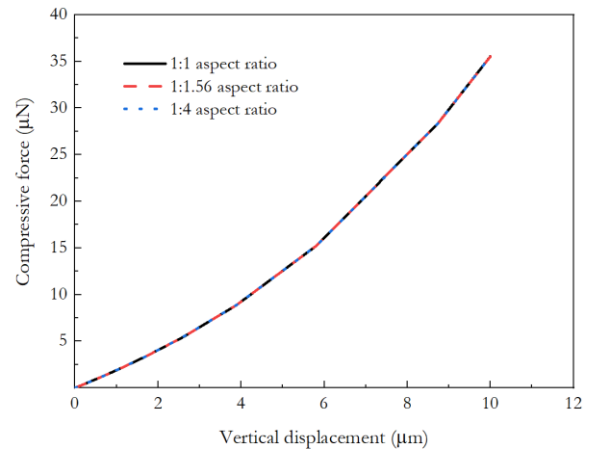


Fig. 11. Plot of compressive force and vertical displacement for various aspect ratio of prism-micropillars.

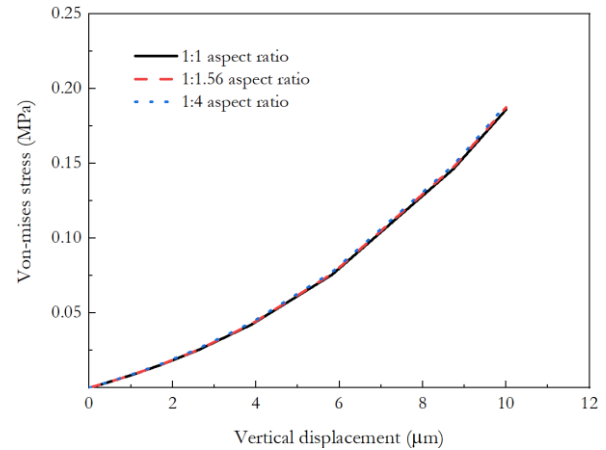
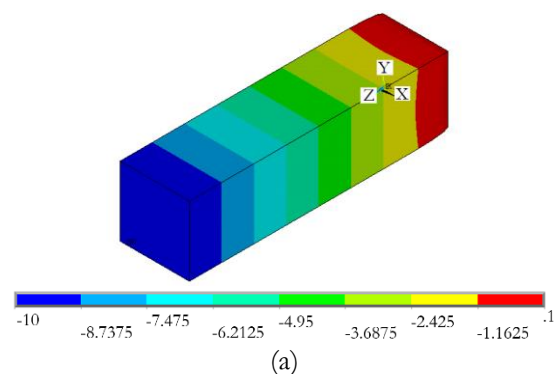


Fig. 12. Plot of von-mises stress and vertical displacement for various aspect ratios of prism-micropillars.



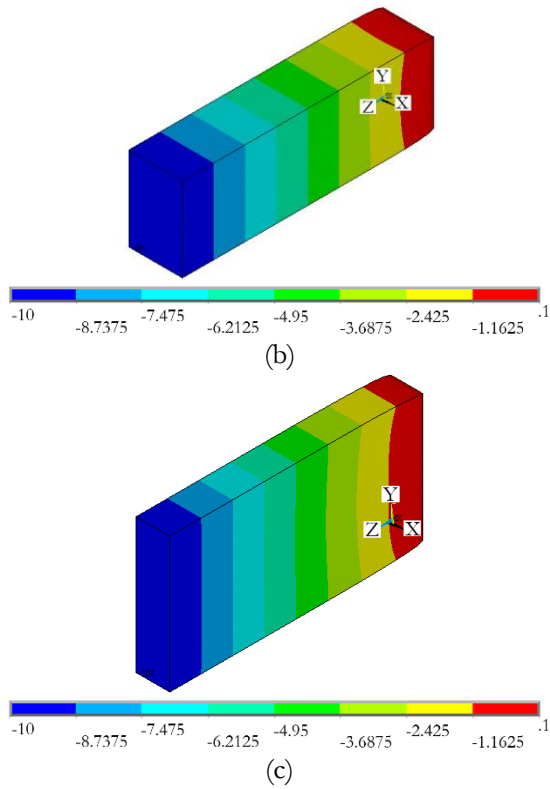


Fig. 13. Contour plot of deformation in the z-direction ( $\mu\text{m}$ ) for aspect ratios of (a) 1:1, (b) 1:1.56 and (c) 1:4.

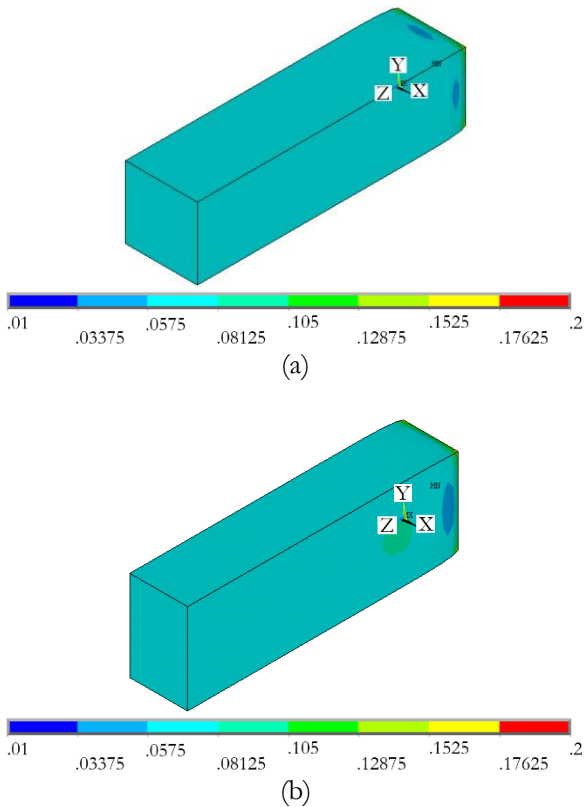


Fig. 14. Contour plot of von-mises stress (MPa) at the displacement  $z = -10 \mu\text{m}$  on the micropillars with (a) 1:1 aspect ratio, (b) 1:1.56 aspect ratio and (c) 1:4 aspect ratio.

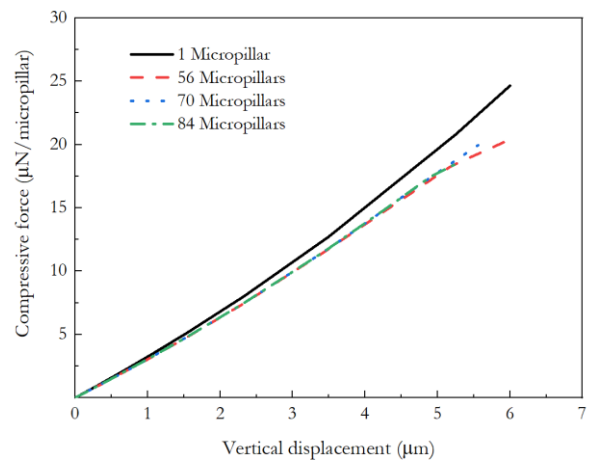


Fig. 15. Plot of compressive force and vertical displacement for F3 pattern.

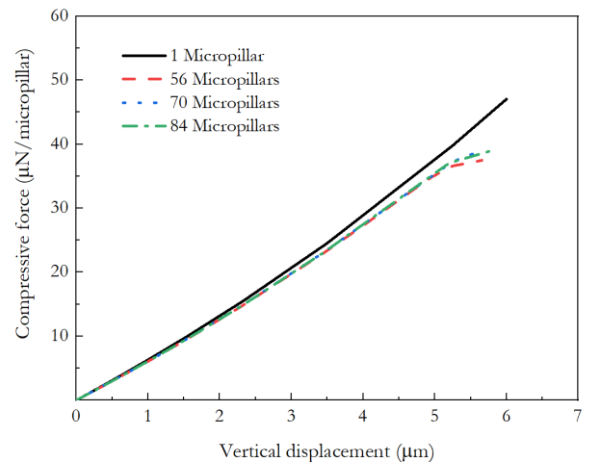


Fig. 16. Plot of compressive force and vertical displacement for F4 pattern.

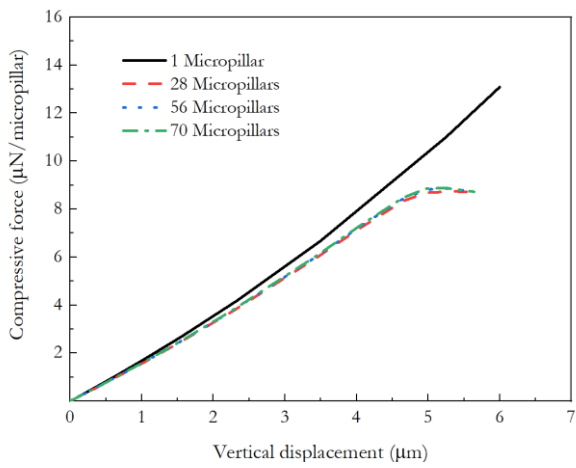


Fig. 17. Plot of compressive force and vertical displacement for F8 pattern.

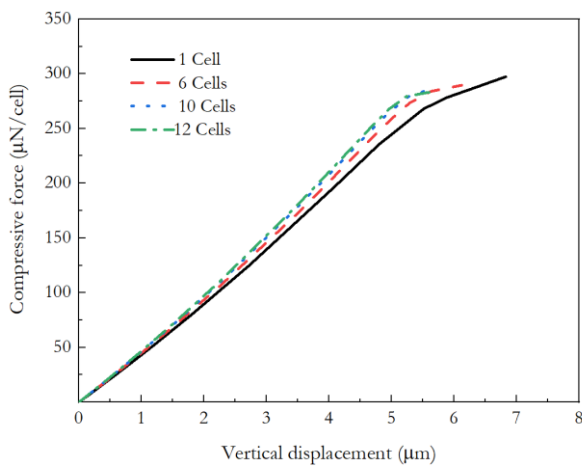


Fig. 18. Plot of compressive force and vertical displacement for F13 pattern.

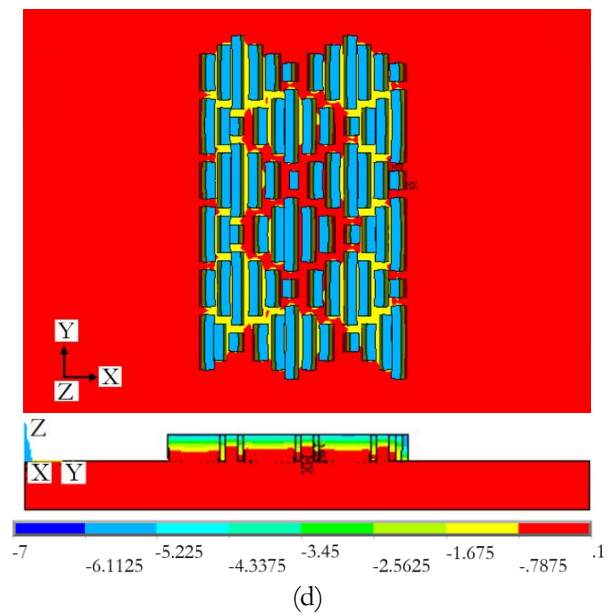
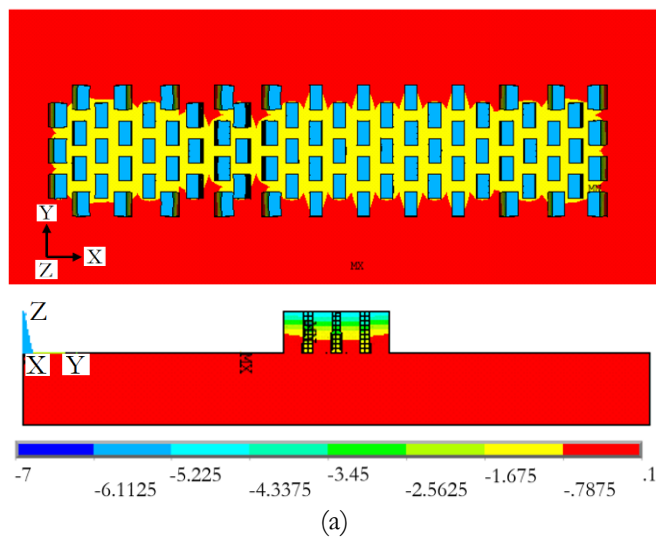
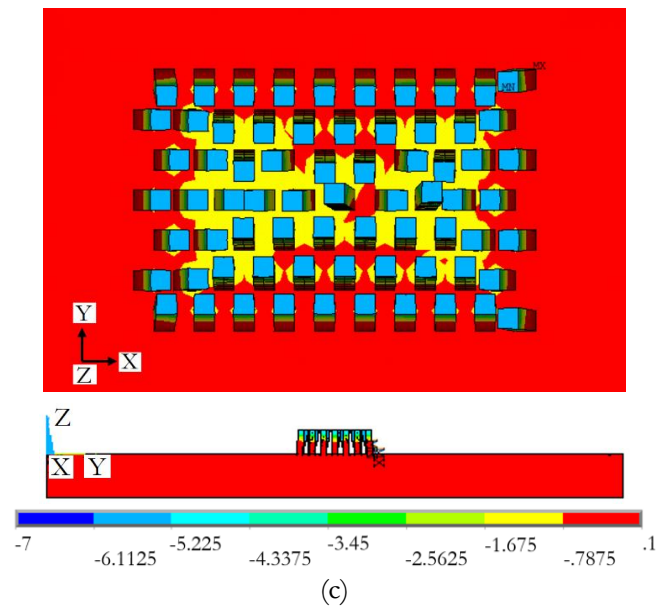
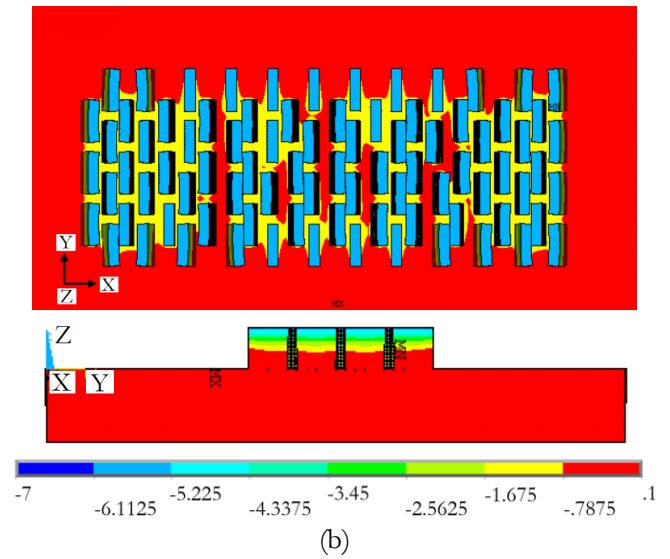


Fig. 19. Contour plot of deformation in the z-direction ( $\mu\text{m}$ ) for (a) F3 pattern, (b) F4 pattern, (c) F8 pattern and (d) F13 pattern.

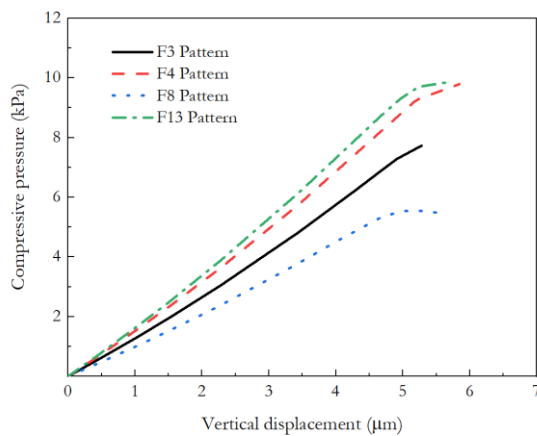


Fig. 20. Plot of compressive pressure and vertical displacement for various micropillar patterns.

## 5. Conclusions

For prism micropillars, the aspect ratio of the rectangular cross-section had not influence on both elastic stiffness and compressive strength. Furthermore, micropillar sheets consisting of F3, F4, F8 and F13 patterns on 150 µm thick substrate were studied on their compressive behaviors. The convergences of the FE results on the FE models of F3 pattern (84 micropillars), F4 pattern (84 micropillars), F8 pattern (70 micropillars) and F13 pattern (12 cells) on the 150 µm thick substrate were found. Here, the maximum compressive pressures of all micropillar patterns were determined as the maximum compressive pressure for which the lateral collapses of micropillars were detected. These compressive pressures were 7.73 kPa (for F3 pattern), 9.79 kPa (for F4 pattern), 5.45 kPa (for F8 pattern) and 9.87 kPa (for F13 pattern). Finally, the F13 pattern has the highest compressive strength but has the lowest WCA. To design such an effective micro-pattern, one has to optimize the loading contact area to achieve both high WCA and loading strength.

## Acknowledgement

This research was supported by Thailand Graduate Institute of Science and Technology, National Science and Technology Development Agency [contract number SCA-CO-2561-7124TH] and National Electronics and Computer Technology Center (NECTEC), Thailand [FlexARs project, grant number P1951452]. The authors acknowledge all staffs at Thai Microelectronics Center (TMEC), for Si mold fabrication and characterization.

## References

- [1] G. D. Bixler and B. Bhushan, "Biofouling: Lessons from nature," *Phil. Trans. R. Soc. A*, vol. 370, pp. 2381-2417, May 2012.
- [2] A. Sabbah, A. Youssef, and P. Damman, "Superhydrophobic surfaces created by elastic instability of PDMS," *Appl. Sci* vol. 6, pp. 152-159, May 2016.
- [3] D. J. C. Gomes, N. C. Souza, and J. R. Silva, "Using a monocular optical microscope to assemble a wetting contact angle analyser," *Measurement*, vol. 46, pp. 3623-3627, Jul. 2013.
- [4] A. M. A. Mohamed, A. M. Abdullah, and N. A. Younan, "Corrosion behavior of superhydrophobic surfaces: A review," *Arabian Journal of Chemistry*, vol. 8, no. 6, pp. 749-765, Nov. 2015.
- [5] W. Bae, M. K. Kwak, H. E. Jeong, C. Pang, H. Jeong, and K. Suh, "Fabrication and analysis of enforced dry adhesives with core-shell micropillars," *Soft Matter*, vol. 9, no.20, pp. 1422-1427, Nov. 2012.
- [6] M. V. Graham, and N. C. Cady, "Nano and microscale topographies for the prevention of bacterial surface fouling," *Coatings*, vol. 4, pp. 37-59, Jan. 2014.
- [7] Y. Rahmawan, S. M. Kang, S. Y. Lee, K. Suh, and S. Yang, "Enhanced shear adhesion by mechanical interlocking of dual-scaled elastomeric micropillars with embedded silica particles," *Macromolecular Reaction Engineering*, vol. 7, no. 10, pp. 616-623, 2013.
- [8] N. Atthi, O. Nimittrakoolchai, S. Supothina, J. Supadech, W. Jeamsaksiri, A. Pankiew, C. Hruanun, and A. Poyai, "An effect of silicon micro-/nano-patterning arrays on superhydrophobic surface," *J. Nanosci. Nanotechnol*, vol. 11, no. 10, pp. 8967-8973, Oct. 2011.
- [9] N. Atthi, W. Sripumkhai, P. Pattamang, O. Thongsook, A. Srihapat, R. Meananeatra, J. Supadech, N. Klunngien, and W. Jeamsaksiri, "Fabrication of robust PDMS micro-structure with hydrophobic and antifouling properties," *Microelectronic Engineering*, vol. 224, Feb. 2020.
- [10] N. Lu, W. Zhang, Y. Weng, X. Chen, Y. Cheng, and P. Zhou, "Fabrication of PDMS surfaces with micro patterns and the effect of pattern sizes on bacteria adhesion," *Food control*, vol. 68, pp. 344-351, Apr. 2016.
- [11] A. Chebolu, B. Laha, M. Ghosh, and Nagahanumaiah, "Engineering of micro patterned surface topographies-correlating pattern geometry and bacterial resistance," in *5th International & 26th All India Manufacturing Technology, Design and Research Conference*, Dec. 2014.
- [12] T. Pakawan, T. Puttapitukporn, N. Atthi, W. Sripumkhai, P. Pattamang, N. Klunngien, and W. Jeamsaksiri, "Compressive behaviors of micropillar sheets made of PDMS material using the finite element method," *Eng. J.*, vol. 24, no. 4, pp. 73-84, Jul. 2020.
- [13] K. Thanakhun and T. Puttapitukporn, "PDMS material models for anti-fouling surfaces using finite element method," *Eng. J.*, vol. 23, no. 6, pp. 381-398, Nov. 2019.
- [14] D. Cheng, S. S. Sridharamurthy, J. T. Hunter, J. S. Park, N. L. Abbott, and H. Jiang, "A sensing device using liquid crystal in a micropillar array supporting structure," *Journal of Microelectromechanical Systems*, vol. 18, no. 5, pp. 973-982, Oct. 2009.

- [15] S. Johari, and L. Y. Shyan, "Stress-strain relationship of PDMS micropillar for force measurement application," in *InCAPE*, 2017.
- [16] D. R. P. Singh, N. Chawla, G. Tang, and Y. L. Shen, "Micropillar compression of Al/SiC nanolaminates," *Acta Materialia*, vol. 58, pp. 6628-6636, Dec. 2010.
- [17] P. Du, I. Lin, H. Lu, and X. Zhang, "Extension of the beam theory for polymer bio-transducers with low aspect ratios and viscoelastic characteristics," *Journal of Micromechanics and Microengineering*, vol. 20, no. 9, Aug. 2010.
- [18] N. E. Oyunbaatar, D. H. Lee, S. J. Patil, E. S. Kim, and D. W. Lee, "Biomechanical characterization of cardiomyocyte using PDMS pillar with microgrooves," *Sensors*, vol. 16, pp. 1258-1270, Aug. 2016.
- [19] C. H. Liu, W. Chen, W. Su, and C. N. Suu, "Numerical and experimental analysis of the automated demolding process for PDMS microfluidic devices with high-aspect ratio micropillars," *International Journal of Advanced Manufacturing Technology*, vol. 80, no. 1-4, pp. 401-409. Mar. 2015.
- [20] T. Xu, J. H. Yoo, S. Babu, S. Roy, J. B. Lee, and H. Lu, "Characterization of the mechanical behavior of SU-8 at microscale by viscoelastic analysis," *Journal of Micromechanics and Microengineering*, vol. 26, no. 10, p. 105001, Aug. 2016.
- [21] M. Shahzad, A. Kamran, M. Z. Siddiqui, and M. Farhan, "Mechanical characterization and FE modelling of a hyperelastic material," *Mat. Res.*, vol. 18, no. 5, pp. 918-924, Jul. 2015.



**Thitikan Pakawan** received the B.Eng. degree in mechanical engineering from Kasetsart University Sriracha Campus in 2016 and she is currently receiving scholarship from Thailand Graduate Institute of Science and Technology (TGIST), National Science and Technology Development Agency (NSTDA).



**Tumrong Puttapitukporn** received the B.Eng. degree in mechanical engineering from Kasetsart University, Thailand in 1998, and the M.S. and Ph.D. degree in mechanical engineering from Oregon State University, USA in 1999 and 2003 respectively.

He is currently the Associate Professor in Department of Mechanical Engineering, Kasetsart University, Thailand. His research focus on finite element modeling and applications of generalized continuum theories.



**Nithi Atthi** received his M.Eng. and Ph.D. in electronics and applied physics from Tokyo Institute of Technology, Japan in 2013 and 2016, respectively.

He has co-authored of 25 technical journal publications, presented his research in 100 conferences and also filed 20 patents. In 2018, he took a position as a research team leader of Surface and Microfluidic Device Innovation Research Team, Thai Microelectronics Center (TMEC), Thailand. His work interest include Si-based semiconductor process technology, micro/nano patterning, high-k/metal gate stacks, microfluidic devices, and superoleophobic surface by surface texturing and modification for various applications



**Witsaroot Sripumkhai** received M.S. degree in science and nanotechnology from College of Nanotechnology, KMUTT, Thailand.

He is currently a Senior Assistant Researcher in Surface and Microfluidic Device Innovation Research Team at Thai Microelectronics Center (TMEC), NECTEC, NSTDA. His research interests Microfabrication process for microfluidic applications and superhydrophobic surface for antifouling application.



**Pattaraluck Pattamang** received M.S. degree in science and nanotechnology from College of Nanotechnology, KMUTT, Thailand.

She is currently an Assistant Researcher in Surface and Microfluidic Device Innovation Research Team at Thai Microelectronics Center (TMEC), NECTEC, NSTDA. Her interests are Microfluidic device and Lab on a disk.



**Nipapan Klunngien** received the B.Eng. degree in electronic engineering from King Mongkut's Institute of Technology Ladkrabang in 1996 and the M.Sc. and Ph.D. degree in microelectronics from University of Newcastle upon Tyne, Newcastle, UK, in 2005.

Since 2005, she is a researcher at Thai Microelectronics Center (TMEC), National Electronics and Computer Technology Center (NECTEC), Thailand. Her research interests are CMOS technology, semiconductor devices, high-k gate dielectrics, and sensor technology.



**Wutthinan Jeamsaksiri** received his M.Eng. and Ph.D. from department of electrical and electronic engineering, Imperial College, London in 1996 and 2003, respectively.

He then worked as a process integration engineer on a European project at IMEC, Leuven, Belgium from 2000 to 2004. The project he carried out was on Integration of Microwave Performance Advanced CMOS Technology. From 2005 he has been working at Thai Microelectronics Center (TMEC) under the National Electronics and Computer Technology Center (NECTEC). In 2018 he took the position as a research group director of TMEC. His work interest includes Si based sensors, MEMS, microfluidic devices, and Surface texturing and modification for various applications.